Available online at www.sciencedirect.com
SCIENCE DIRECT
Journal of Photochemistry and Photobiology A: Chemistry 176 (2005) 107–113
Journal of Photochemistry and Photobiology A:Chemistry
www.elsevier.com/locate/jphotochem

Wavelength dependent photodissociation of CH_3OOH Quantum yields for CH_3O and OH, and measurement of the OH + CH_3OOH rate coefficient

Mark A. Blitz, Dwayne E. Heard *, Michael J. Pilling

School of Chemistry, University of Leeds, Leeds LS2 9JT, UK

Available online 28 October 2005

Abstract

Methyl hydroperoxide, CH_3OOH, has been synthesised with >99.5% purity, confirmed using UV absorption spectroscopy and high-pressure liquid chromatography (HPLC) followed by post-column derivatisation. The UV absorption cross-section for CH_3OOH was measured and for <325 nm was in good agreement with the literature. Laser-flash photolysis combined with laser-induced fluorescence (LIF) spectroscopy has been used to measure both OH and CH_3O photofragments following the photolysis of CH_3OOH in the wavelength range 223–355 nm. Using the previously measured unity quantum yield for OH at 248 nm as a reference, the LIF signals immediately following photolysis were used to measure wavelength dependent quantum yields for OH and CH_3O, taking into account changes in laser pulse energy and absorption cross-section. The quantum yields for both species were unity within experimental error. The rate coefficient for the reaction of OH with CH_3OOH (R1a) to generate $CH_3O_2 + H_2O$ products was measured at 295 K to be $k_{(R1a)} = (9.0 \pm 0.2) \times 10^{-12}$ cm^3 molecule^{-1} s^{-1}, considerably higher (by about a factor of two) than previous values measured by Vaghjiani and Ravishankara [G.L. Vaghjiani, A.R. Ravishankara, J. Phys. Chem. 93 (1989) 1948–1959] and Niki et al. [H. Niki, P.D. Maker, C.M. Savage, L.P. Breitenbach, J. Phys. Chem. 87 (1983) 2190–2193].

Keywords: Wavelength dependent photolysis; Kinetics; Peroxides; Hydroxyl radicals; Laser-induced fluorescence; Atmospheric chemistry; HO_x radicals; Methoxy radical; Rate coefficient

1. Introduction

The majority of oxidation in the atmosphere is initiated by the hydroxyl radical, OH. Two of the largest losses of OH are by reaction with CO and CH_4, which generate the peroxy radicals, HO_2, and CH_3O_2:

$$OH + CO \rightarrow H + CO_2 \quad \text{followed by}$$
$$H + O_2 + M \rightarrow HO_2 + M$$

$$OH + CH_4 \rightarrow CH_3 + H_2O \quad \text{followed by}$$
$$CH_3 + O_2 + M \rightarrow CH_3O_2$$

Peroxy radicals in the atmosphere are removed either by reaction with O_3, NO or by self- and cross-recombination reactions, with the latter being the dominant pathway in clean air, forming peroxides:

$$HO_2 + HO_2 \rightarrow H_2O_2 + O_2$$

$$HO_2 + CH_3O_2 \rightarrow CH_3OOH + O_2$$

Peroxides are, therefore, indicators of chemical processing in the troposphere, as they are formed from peroxy radicals, which are the result of oxidation of VOCs by OH, NO_3 or O_3. Hydrogen peroxide is also an efficient oxidant in cloud droplets converting SO_2 into sulphuric acid, H_2SO_4 [3]. Peroxides act as reservoirs of other oxidants, as they are photolysed by sunlight near-UV wavelengths, releasing radicals:

$$H_2O_2 + h\nu \rightarrow OH + OH, \quad \lambda_{\text{threshold}} = 556\,\text{nm}$$

$$CH_3OOH + h\nu \rightarrow CH_3O + OH, \quad \lambda_{\text{threshold}} = 618\,\text{nm}$$

$$\text{followed by } CH_3O + O_2 \rightarrow HO_2 + CH_2O$$

* Corresponding author. Tel.: +44 113 343 6471; fax: +44 113 343 6565.
E-mail address: d.e.heard@leeds.ac.uk (D.E. Heard).

1010-6030/$ – see front matter © 2005 Elsevier B.V. All rights reserved.
doi:10.1016/j.jphotochem.2005.09.017

However, if peroxides react with OH or are lost by rainout or dry deposition to the surface, they become a sink for free radicals:

$$OH + H_2O_2 \rightarrow \text{products}$$

$$OH + CH_3OOH \rightarrow \text{products} \quad \text{(R1)}$$

Peroxides have been measured in the troposphere and free-troposphere using a variety of instruments on ground-based and aircraft platforms [4–7]. Measurements are common for H_2O_2 and CH_3OOH, but quite rare for the more complex organic peroxides. In clean air, typical H_2O_2 concentrations vary from a few hundred parts per trillion (ppt) up to ca. 1 part per billion (ppb), but concentrations up to several ppb are not uncommon in more polluted air. For the organic peroxides, with CH_3OOH constituting the majority, concentrations are typically 50% of H_2O_2 [5].

As mentioned above peroxides can act as both sources and sinks of OH. During the Southern Ocean Photochemistry Experiment (SOAPEX 2), held at Cape Grim, Tasmania in 1999, photolysis of H_2O_2 and CH_3OOH constituted on average 4% and 2%, respectively of the total OH production, whereas the reaction OH + CH_3OOH constituted 5% of the total loss of OH [8]. In the boundary layer, the photolysis of peroxides is a relatively minor source of OH, as OH production is dominated by ozone photolysis to generate $O(^1D)$ atoms, followed by the reaction of $O(^1D)$ with water vapour. However, in the upper troposphere (UT), the concentration of water vapour is much smaller, and convective transport of H_2O_2 and CH_3OOH may inject significant concentrations in the UT, leading to a significant source of OH following photolysis, although a significant fraction of H_2O_2 may be scavenged in clouds by washout [9]. During the PEM-Tropics, a mission over the South Pacific, photolysis of peroxides was found to be a major source (35%) of OH during convective events [10–12]. However, OH levels were not enhanced significantly because of the increased sink from reaction with transported CH_3OOH.

For both peroxides, the absorption cross-sections drop off rapidly at wavelengths above the actinic cut-off at 290 nm, but photolysis still represents a significant loss process for both species. The photochemistry of H_2O_2 has been the focus of many experimental and theoretical studies [13–17]. The ultraviolet absorption spectrum of H_2O_2 is continuous over the region 106–350 nm [14], indicating a short-lived and purely dissociative excited state, with an OH quantum yield of two measured for >222 nm [15]. However, the absorption cross-section and photodissociation quantum yields for CH_3OOH have been the subject of fewer studies. Vaghjiani and Ravishankara [14,15] have determined the absorption cross-section of CH_3OOH between 210 and 360 nm and have measured the quantum yield for OH formation to be 1 ± 0.18 at 248 nm under bulb conditions. Similarly, Thelen et al. [18] showed that CH_3OOH exclusively photofragments to form CH_3O and OH after excitation at 193 and 248 nm under molecular beam conditions.

The reaction between OH and CH_3OOH has two potential product channels:

$$OH + CH_3OOH \rightarrow CH_3O_2 + H_2O \quad \text{(R1a)}$$

$$\rightarrow CH_2OOH + H_2O \quad \text{(R1b)}$$

where CH_2OOH is unstable and rapidly falls apart (on a microsecond timescale, see Section 3.3 for further discussion) to regenerate OH:

$$CH_2OOH + M \rightarrow CH_2O + OH + M$$

Only two kinetics studies of reaction (R1) have been performed. Niki et al. [2] determined a value of $k_{(R1)} = k_{(R1a)} + k_{(R1b)} = 1.0 \times 10^{-11}$ cm^3 molecule^{-1} s^{-1} in an FTIR end-product analysis chamber experiment at 298 K, where $k_{(R1)}$ was measured relative to OH + C_2H_4 and OH + CH_3CHO. The branching ratio $k_{(R1a)}/k_{(R1b)}$ was found to be 1.3 ± 0.26. Vaghjiani and Ravishankara [1], who monitored the temporal behaviour of OH, ^{18}OH and OD using laser-induced fluorescence (LIF) in the presence of CH_3OOH, obtained a value of $k_{(R1)} = (5.38 \pm 0.44) \times 10^{-12}$ cm^3 molecule^{-1} s^{-1} and a branching ratio of $k_{(R1a)}/k_{(R1b)} = 2.52 \pm 0.36$.

In the present study we have synthesised CH_3OOH, and using a combination of UV–vis absorption spectroscopy and high-pressure liquid chromatography (HPLC) have shown that sample is very pure. The photolysis of CH_3OOH at a range of wavelengths is studied by measuring *both* the OH and CH_3O radical photofragments using laser-induced fluorescence, from which it is shown that under all conditions the excited state is purely dissociative, giving a quantum yield of one. The purity of the sample and the monitoring of both products are important, as the most likely contaminant in the synthesis of CH_3OOH is H_2O_2. Using laser-flash photolysis followed by time-resolved LIF to monitor decays of OH in the presence of a range of CH_3OOH concentrations, we have measured $k_{(R1a)}$ at room temperature.

2. Experimental

2.1. Preparation of methyl hydroperoxide, CH_3OOH

Methyl hydroperoxide, CH_3OOH, is not commercially available. Consequently, it was prepared by the methylation of hydrogen peroxide, closely following the procedure described by Vaghjiani and Ravishankara [1]. Attention is drawn to the caution given during the description of this procedure [1], regarding the potential explosive nature of residues when they are exposed to air. The resulting CH_3OOH in the aqueous phase was transferred into diethyl ether (DEE) using continuous liquid/liquid extraction over a number of hours. The ether solution was dried with sodium sulphate and then concentrated by boiling off the ether at 308 K. The two potential impurities in the sample are diethyl ether, the solvent used to extract the peroxide, and H_2O_2. The former has a large vapour pressure and is readily removed by pumping on the peroxide sample in dry ice; the latter has a much smaller vapour pressure than CH_3OOH and is, therefore, readily separated by the distillation of CH_3OOH. The resulting CH_3OOH was transferred to ~1 g sample bottles (only 1 g was made at a time) and stored in a freezer at −18 °C.

The purity of the CH_3OOH was determined using reverse phase high-pressure liquid chromatography with post-column derivatisation via the peroxidase enzyme fluorescence method of Lazrus and co-workers [4,19]. Separation on a C-18 reverse phase column is followed by derivatisation to form the stable dimer of *p*-hydroxyphenylacetic acid (*p*-HAA) by addition of the reagent horseradish peroxidase in buffered potassium hydrogen phthalate. The pH was then raised to convert the dimer into its fluorescent anionic form allowing quantification by fluorescence. The analytical technique is able to separate H_2O_2 from CH_3OOH and higher organic peroxides (producing distinct chromatographic peaks), and CH_3OOH was observed to be >99.5% of the peroxides present in the sample, with H_2O_2 and CH_3OOCH_3 being the minor constituents.

Prior to use, the CH_3OOH in the sample bottle was transferred to a vacuum line and subjected to several freeze–pump–thaw cycles before being transferred either to an absorption cell (10 cm in length) or to a 5 l bulb for dilution in helium for immediate use in photodissociation and kinetics experiments. UV–vis absorption spectra were recorded with a laboratory spectrometer (Perkin Elmer Lambda 900).

2.2. Photolysis and kinetics experiments

The apparatus used is a slight modification of the slow flow, laser-flash photolysis/LIF technique, which has been previously described [20]. Photolysis of CH_3OOH was achieved in one of four ways: (i) by the 248 nm output from an excimer laser (Lambda Physik, Minex); (ii) by the frequency-doubled output; or (iii) the frequency-doubled and sum-frequency mixed output from a Nd:YAG (Spectron, SL803) pumped dye laser (Spectron, SL4000), using an appropriate dye; and (iv) the third harmonic of the Nd:YAG laser for photolysis at the longer wavelength of 355 nm. Photolysis at 248 nm was used as a reference wavelength (see below) and the laser beam at this wavelength counter-propagated the laser beam of the other photolysis wavelengths through the reaction cell, which was a six-way cross. The spatial cross-sections of the photolysis laser beams (248 nm or other wavelengths, used alternatively) were controlled using irises so that they defined the same volume in the reaction zone. The output energy from the Nd:YAG pumped dye laser was typically a few mJ per pulse, and the pulse energy of the excimer laser was adjusted to give a comparable amount of photolysis at 248 nm. The energy of the lasers was determined by averaging the output of an energy meter (Gentec EDL 200) over typically 50 laser pulses. The OH photofragment was probed using off-resonant LIF via the $A^2\Sigma^+$ ($v' = 1$) $\leftarrow X^2\Pi_i$ ($v'' = 0$), $Q_1(1)$ transition at 281.913 nm, and the CH_3O photofragment probed using off-resonant LIF via the A^2A_1 ($v'_{CO} = 3$) $\leftarrow X^2E_1$ ($v''_{CO} = 0$) transition at 292.8 nm [21,22], both in combination with a 305-nm long-pass filter (Schott WG-305). The probe wavelengths were generated using the frequency-doubled output from a Nd:YAG (Spectra Physics, Quanta-Ray GCR150) pumped dye laser (Spectra Physics, Quanta-Ray PDL-3, Rhodamine 6 G for 281.9 nm and Rhodamine B for 292.8 nm). The probe beam was unfocussed and entered the reaction cell at right angles to either of the photolysis lasers, and the beam-overlap region was ~1.5 cm in diameter. Perpendicular to the plane containing the laser beams were two convex lenses ($f = 4.0$ cm), mounted inside the reaction cell, and used to image the OH or CH_3O fluorescence. The lenses were arranged to image the reaction zone through an iris to match the diameter of the probe laser, and through the long-pass filter onto a photomultiplier (PMT, EMI 9813). The PMT signal was integrated with a boxcar averager (SRS), which was adjusted to exclude the first 50 ns of the signal following the photolysis laser pulse, and digitised before transfer to a personal computer for subsequent data analysis. The delay between the photolysis and probe lasers was changed by a delay generator (SRS 535) under computer control, and the temporal evolution of OH or CH_3O following the photolysis was recorded at ~100 delays, with each data point averaged over four–eight laser shots.

Mass flow controllers (MKS) were used to adjust the flow of CH_3OOH and helium, the buffer gas used. The pressure in the photolysis cell was measured using capacitance manometers (MKS) and adjusted between 10 and 400 Torr by throttling the exit valves on the cell. The total flow rate, combined with a pulse-repetition-frequency of all the lasers of 5 Hz, ensured a fresh sample of gas was photolysed by each subsequent laser pulse and the cell was maintained at 295 K. Helium (BOC, CP grade, 99.999%) was used from the cylinder without further purification.

3. Results and discussion

3.1. UV–vis absorption spectrum of CH_3OOH

Typically, 20 Torr of CH_3OOH was transferred from the vacuum line into the 10 cm absorption cell, which was placed into the UV–vis spectrometer. However, it was difficult to position the absorption cell exactly in the same place between runs (for example, between using a cell containing CH_3OOH and an empty cell), and hence a small but discernable baseline was present, especially at longer wavelengths above 320 nm where the emission lamps in the spectrometer change, and hence it was only possible to measure absorption cross-sections above $\sim 10^{-21}$ cm^2 molecule^{-1}, corresponding to $(I - I_0)/I_0 \sim 0.005$. Fig. 1 shows an absorption spectrum of CH_3OOH measured over the range 225–360 nm together with that measured by Vaghjiani and Ravishankara [14], and Table 1 lists the measured cross-sections. The spectra agree within 30% in the range 225–325 nm, but beyond 325 nm our values become too high, ascribed to the baseline problem mentioned above. For $\lambda < 325$ nm, the good agreement with the literature, taken together with the high purity (>99.5%) measured using the HPLC method, gives us confidence that our sample is indeed CH_3OOH.

However, our values for σ_{CH_3OOH} are unreliable above 320 nm and in Table 1 no values are given above this wavelength.

3.2. Photodissociation quantum yields

Examples of time-profiles of OH and CH_3O radicals following the photolysis of CH_3OOH are given in Figs. 2 and 3,

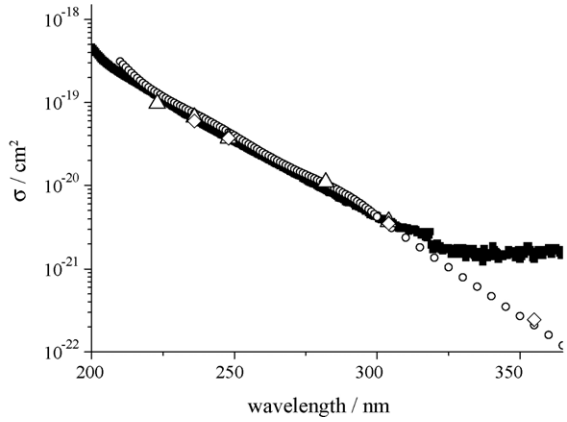

Fig. 1. Filled squares: UV absorption spectrum of CH_3OOH recorded using ~20 Torr of CH_3OOH in a 10 cm cell. Open circles: absorption spectrum measured by Vaghjiani and Ravishankara [14]. The measured quantum yields for CH_3O (open triangles) and OH (open diamonds) were also used to calculate the cross-sections at specific wavelengths (see text for details).

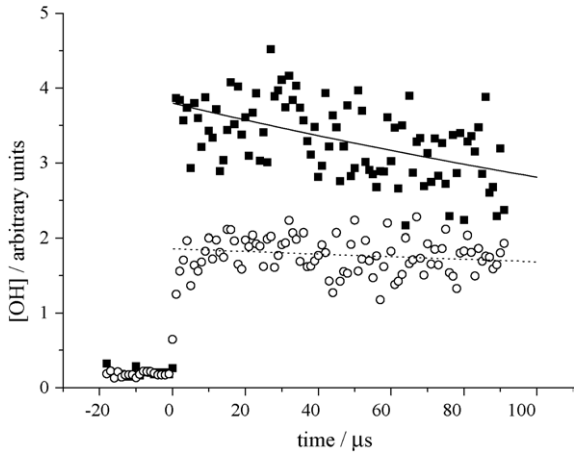

Fig. 2. OH LIF signal observed following the photolysis (at $t = 0$) of CH_3OOH at 355 nm (open circles, 3.6 mJ per laser pulse) and 248 nm (filled squares, 0.52 mJ laser pulse), recorded at a total pressure of 74 Torr helium.

respectively. Vaghjiani and Ravishankara [15] and Thelen et al. [18] showed that the 248 nm photolysis of CH_3OOH gave exclusively CH_3O and OH with a quantum yield of one. We have used this result as our reference and assign the LIF signal at 248 nm for both species as equivalent to a quantum yield of one, in order to compare with the signal at other wavelengths. The time-profiles were fitted to the following exponential decay:

$$[RO] = [RO]_0 \exp(-k'_{(R1)}t) \quad \text{(E1)}$$

where $[RO]_0$ is the initial radical concentration, R = H or CH_3, and $k'_{(R1)}$ is the pseudo-first-order rate constant for the loss of RO, given by:

$$k'_{(R1)} = k_{(R1)}[CH_3OOH] + k_{diffusion} \quad \text{(E2)}$$

Table 1
UV absorption cross-sections for CH_3OOH at 295 K

Wavelength (nm)	This work	Vaghjiani and Ravishankara [14]
	σ (10^{-20} cm^2 molecule^{-1})	
210	22.7	31.2
220	14.0	15.4
230	8.40	9.62
240	5.27	6.05
250	3.42	3.98
260	2.25	2.56
270	1.47	1.70
280	0.956	1.09
290	0.624	0.691
300	0.429	0.413
310	0.307	0.239
320	0.200	0.137
330	[a]	0.079
340	[a]	0.047
350	[a]	0.027
355	[a]	0.021

[a] We do not report values above 320 nm due to the presence of a baseline associated with the difficulty in positioning the absorption cell precisely in the same place between background and sample runs, which is exacerbated at 329 nm where the source lamps in the spectrometer change.

with $k_{diffusion}$ representing the diffusive loss of RO out of the overlap region between the two laser beams. For the photodissociation quantum yield experiments typically 10 mTorr of CH_3OOH was photolysed in the presence of 75 Torr of He (although the pressure of each was varied in some experiments), and the time-profiles were only recorded out to a few tens of microseconds as only $[RO]_0$ is required. Time-profiles were recorded for a variety of photolysis wavelengths, and in every case, the time-profile for the reference wavelength of 248 nm was also recorded within 5 min. The energies of the photolysis laser pulses were adjusted, using neutral density filters, to maintain a similar LIF signal radical at 248 nm and the other wavelength, as shown for OH and CH_3O in Figs. 2 and 3, respectively. The rise-time was very rapid compared with the decay rate, and the initial concentration at $t = 0$ (which is proportional to the initial LIF signal) was obtained by fitting a falling exponential function to the data and extrapolating to $t = 0$. The ratio of the quantum yields at the two wavelengths is linked to the ratio of the two

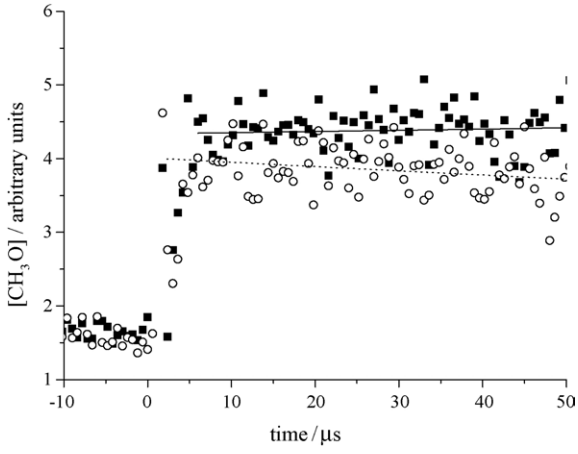

Fig. 3. CH_3O LIF signal observed following the photolysis (at $t = 0$) of CH_3OOH at 248 nm (open circles, 4.9 mJ) and 282 nm (filled squares, 1.52 mJ) at a total pressure of 52 Torr helium.

Table 2
Quantum yields for OH and CH_3O following photolysis of CH_3OOH

Wavelength (nm)	Quantum yield for CH_3O	Quantum yield for OH
223	0.81 ± 0.12	[a]
236	1.05 ± 0.16	0.95 ± 0.14
248	1	1
282	1.09 ± 0.16	[a]
304	1.00 ± 0.15	0.95 ± 0.14
355	[a]	1.19 ± 0.18

The values are all scaled to a value of unity obtained for OH at 248 by Vaghjiani and Ravishankara [15] and Thelen et al. [18].
[a] Not measured.

initial concentrations, $[RO]_0$, by the expression:

$$\frac{\phi_{RO,\lambda}}{\phi_{RO,248}} = \frac{[RO]_\lambda}{[RO]_{248}} \frac{N_{248}}{N_\lambda} \frac{\sigma_{248}}{\sigma_\lambda} \quad \text{(E3)}$$

where N is the number of photons per laser pulse (determined from an average of $\geq$50 shots) and σ is the absorption cross-section, which is listed in Table 1. The rate of electronic quenching of the OH or CH_3O fluorescence is the same at the two wavelengths, as the conditions of pressure and composition are identical, and hence this effect cancels in Eq. (E3) and is not required. At the reference wavelength of 248, $\phi_{RO,248} = 1.0$ [15,18], and therefore, Eq. (E3) reduces to:

$$\phi_{RO,\lambda} = \frac{[RO]_\lambda}{[RO]_{248}} \frac{N_{248}}{N_\lambda} \frac{\sigma_{248}}{\sigma_\lambda} \quad \text{(E4)}$$

from which $\phi_{RO,\lambda}$ was calculated from the ratio of the initial LIF signals at the two wavelengths, the measured laser-energies and the tabulated cross-sections obtained by Vaghjiani and Ravishankara [14]. The quantum yields for both OH and CH_3O obtained in this manner are summarised in Table 2. The uncertainty in the value of $\phi_{RO,\lambda}$ is estimated as 15%, and is mainly due to the error in $[RO]_\lambda/[RO]_{248}$, reflecting the ability to maintain a constant spatial overlap of the photolysis and probe laser beams for the two photolysis wavelengths. With the exception of ϕ_{OH} at 223 nm, the quantum yields measured in this work are unity within experimental error. Rearranging Eq. (E4) gives:

$$\frac{\sigma_\lambda}{\sigma_{248}} = \frac{[RO]_\lambda}{[RO]_{248}} \frac{N_{248}}{N_\lambda} \frac{1}{\phi_{RO,\lambda}} \quad \text{(E5)}$$

and hence

$$\sigma_\lambda = \frac{[RO]_\lambda}{[RO]_{248}} \frac{N_{248}}{N_\lambda} \frac{1}{\phi_{RO,\lambda}} \sigma_{248} \quad \text{(E6)}$$

Fig. 1 also shows the values of σ_λ calculated using (E6) for both OH and CH_3O plotted on the same graph as the measured absorption cross-section, and is an alternative way to show that ϕ_{OH} and ϕ_{CH_3O} are very close to one at all wavelengths studied. The other dissociative pathways:

$$CH_3OOH + h\nu \rightarrow CH_3OO + H, \quad \lambda_{threshold} = 324\,nm$$

$$CH_3OOH + h\nu \rightarrow CH_3 + HO_2, \quad \lambda_{threshold} = 403\,nm$$

$$CH_3OOH + h\nu \rightarrow CH_3OH + O(^1D), \quad \lambda_{threshold} = 314\,nm$$

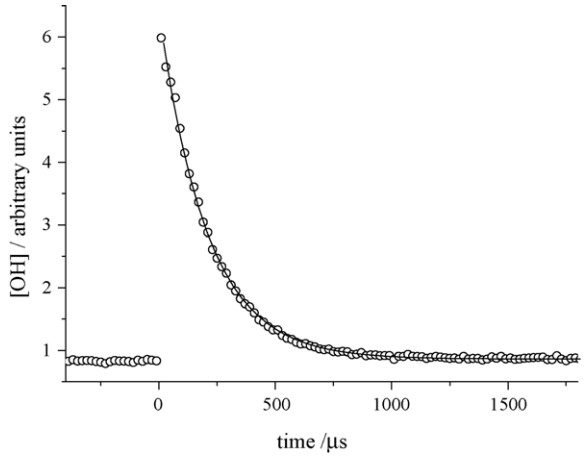

Fig. 4. Decay of OH LIF signal following the photolysis (at $t = 0$) of 16.4 mTorr CH_3OOH at 100 Torr total pressure (helium). The solid line is linear least-squares fit of Eq. (E1) to the data. Note the considerably longer times on the x-axis compared with Figs. 2 and 3.

do not appear important. The quantum yields were insensitive to a change in total pressure in helium up to 400 Torr, suggesting that collisional quenching of the electronically excited CH_3OOH does not compete with dissociation to form OH and CH_3O.

3.3. Measurement of the rate coefficient for the reaction $OH + CH_3OOH$

OH radicals were generated by the 248 nm photolysis of CH_3OOH using He as the buffer gas, at a total pressure of 100 Torr. The 248 nm pulse energy was ~1 mJ so that the OH concentration was kept below 10^{11} molecule cm^{-3}, whereas the concentration of CH_3OOH was varied over the range 2–25 mTorr ($6.5–81 \times 10^{13}$ molecule cm^{-3}), to ensure pseudo-first-order conditions. Time-profiles of OH were recorded over much longer time-periods compared with the photolysis experiments so that the decay of OH by reaction with CH_3OOH could be followed. A typical OH decay is shown in Fig. 4, with the loss of OH primarily due to reaction (R1):

$$OH + CH_3OOH \rightarrow CH_3O_2 + H_2O \quad \text{(R1a)}$$

$$\rightarrow CH_2OOH + H_2O \quad \text{(R1b)}$$

If the decomposition of CH_2OOH to give $OH + CH_2O$ is very rapid on the timescale of the OH decay (see below for further discussion of this point), then measuring the decay of OH will only yield information on reaction (R1a). The OH concentration is given by:

$$[OH] = [OH]_0 \exp(-k'_{(R1)}t) \quad \text{(E1)}$$

$$k'_{(R1)} = k_{(R1)}[CH_3OOH] + k_{diffusion} \quad \text{(E2)}$$

All OH decays were found to follow purely exponential behaviour, as shown by a fit of (E1) to the data also shown in Fig. 4. The rise-time of the OH is instantaneous on the timescale of the decay (see also Fig. 1), and in agreement with Vaghjiani and Ravishankara [1], we see no evidence for production of vibrationally excited OH. Values of $k'_{(R1)}$ were obtained

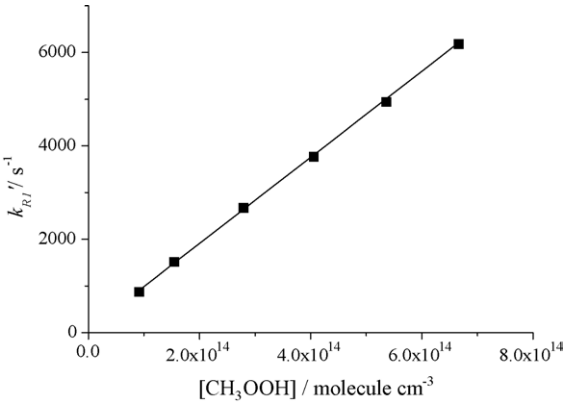

Fig. 5. Plot of the pseudo-first-order rate constant $k'_{(R1)}$ vs. the concentration of CH_3OOH, from which the linear least-squares gradient yields $k_{(R1a)} = (9.0 \pm 0.2) \times 10^{-12}$ cm^3 molecule^{-1} s^{-1} at 295 K.

in this manner for a range of CH_3OOH concentrations, and are shown in Fig. 5. The gradient of $k'_{(R1)}$ versus [CH_3OOH] yielded $k_{(R1a)} = (9.0 \pm 0.2) \times 10^{-12}$ cm^3 molecule^{-1} s^{-1}, at 295 K, with the errors representing both 95% confidence limits of the best linear-fit and the uncertainty in determining [CH_3OOH]. The small intercept in Fig. 5 is consistent with the value of $k_{\text{diffusion}}$ representing diffusion of OH out of the probe laser beam.

Identification of the gradient of Fig. 5 as $k_{(R1a)}$ hinges on the CH_2OOH formed in channel (R1b) falling apart to reform OH on a timescale that is short compared with the observed decay of OH. In the study of OH + CH_3OOH by Vaghjiani and Ravishankara [1], the lifetime of CH_2OOH with respect to decomposition at 205 K and in 50 Torr He was estimated to be <20 μs, based on a comparison of modelled and measured OH decays. At 295 K the rate of CH_2OOH decomposition to reform OH (and CH_2O) will likely be faster, and hence the assumption that the measurement of OH loss in our experiment yields $k_{(R1a)} = (9.0 \pm 0.2) \times 10^{-12}$ cm^3 molecule^{-1} s^{-1} seems justified. To determine the rate coefficient for the overall OH + CH_3OOH reaction, $k_{(R1a)} + k_{(R1b)}$, and the branching ratio, requires measurement of both channels, and was performed by Vaghjiani and Ravishankara [1] using isotopic substitution of the OH reagent (^{16}OH, ^{18}OH and ^{16}OD).

Our value for $k_{(R1a)}$ is over a factor of two greater than the value of $k_{(R1a)} = (3.85 \pm 0.42) \times 10^{-12}$ cm^3 molecule^{-1} s^{-1} obtained by Vaghjiani and Ravishankara [1]. Initially, diethyl ether, the solvent used in the preparation and extraction of CH_3OOH, was considered as a potential contaminant because its rate coefficient with OH is higher ($k_{\text{OH + DEE}} = 1.3 \times 10^{-11}$ cm^3 molecule^{-1} s^{-1} [23–25]). However, this explanation is ruled out on the basis that DEE does not contribute to the observed absorption spectrum above 210 nm [26] and that the use of several freeze–pump–thaw cycles when making up dilute sample bulbs of CH_3OOH should remove DEE effectively. The results of some of our earlier attempts to prepare CH_3OOH and measure $k_{(R1a)}$ are instructive at this point. Preliminary attempts to synthesis CH_3OOH led to lower values of $k_{(R1a)}$ being measured, for example, as low as 3×10^{-12} cm^3 molecule^{-1} s^{-1}, but subsequent analysis of the preliminary sample of CH_3OOH using the HPLC method with post-column derivatisation (using the peroxidase enzyme fluorescence method of Lazrus and co-workers [4,19]) revealed that it contained a large amount (57%) of H_2O_2. The rate coefficient for OH + H_2O_2 is $k_{\text{OH+H}_2\text{O}_2} = 1.7 \times 10^{-12}$ cm^3 molecule^{-1} s^{-1} [13], and hence the presence of significant H_2O_2 contaminant provided an explanation for the lower value obtained for $k_{(R1a)}$. However, once the synthesis and extraction/purification of CH_3OOH had been perfected, >99.5% of the peroxide present in the sample was CH_3OOH (measured using HPLC); and the higher value of $k_{(R1a)}$ was obtained.

In a chamber experiment using FTIR end-product analysis, Niki et al. [2] indirectly measured $k_{(R1)}$ relative to OH + C_2H_4 and OH + CH_3CHO, and obtained a value of $k_{(R1)} = 1.0 \times 10^{-11}$ cm^3 molecule^{-1} s^{-1} at 298 K. Niki et al. [2] also determined $k_{(R1a)}/k_{(R1b)} = 1.30 \pm 0.26$ (compared with 2.52 ± 0.36 determined by Vaghjiani and Ravishankara [1]), and so $k_{(R1a)} = 5.65 \times 10^{-12}$ cm^3 molecule^{-1} s^{-1}, which is 60% lower than our value. Although the experiments of Niki et al. were performed in air, rather than helium, Vaghjiani and Ravishankara [1] showed that the presence of O_2 did not change the rate coefficient. The reason for our higher value of $k_{(R1a)}$ is unknown. The experiments of Vaghjiani and Ravishankara were very carefully performed, with concentrations of CH_3OOH determined immediately prior to admission of the reaction cell using a UV absorption cell (although the UV absorption spectrum and cross-section for CH_3OOH and H_2O_2 are similar). We did not determine [CH_3OOH] immediately before our reaction cell in this manner, and hence although our sample was proven to be extremely pure (>99.5%) we cannot rule out some decomposition, and hence loss of CH_3OOH, in the sample lines between the storage bulb and the reaction cell. However, loss of CH_3OOH would result in a smaller value of $k_{(R1a)}$ compared with the true value. It is acknowledged, however, that decomposition of CH_3OOH on the walls of the sample lines could lead to the formation of an impurity that reacts with OH considerably faster than does CH_3OOH, but given that the measured rate coefficient is ~10^{-11} cm^3 molcule^{-1} s^{-1}, the concentration of impurity compared to CH_3OOH must be significant. We did not investigate the use of different materials for the flow-lines used to introduce the CH_3OOH into the reaction cell and so this possibility cannot be ruled out.

4. Conclusions

Methyl hydroperoxide, CH_3OOH, was synthesised using the methylation of H_2O_2, and its purity found to be >99.5% using UV spectroscopy and HPLC with post-column derivatisation using the peroxidase enzyme fluorescence method. CH_3OOH was photolysed over the wavelength range 223–355 nm and laser-induced fluorescence was used to detect both OH and CH_3O photofragments. Using a reference wavelength of 248 nm, for which the absolute quantum yield for OH had previously been determined to be unity, we have shown, for the first time, that the quantum yield for both OH and CH_3O production is unity across this range of wavelengths, indicating that dissociation is the exclusive fate of CH_3OOH following electronic excitation, even at 355 nm. Photolysis of CH_3OOH

at 248 nm was used as a source of OH to study the kinetics of the $OH + CH_3OOH$ reaction, and the rate coefficient for formation of $CH_3O_2 + H_2O$ products was determined to be $k_{(R1a)} = (9.0 \pm 0.2) \times 10^{-12}\,cm^3\,molecule^{-1}\,s^{-1}$ at 295 K. The value is considerably larger than previously measured values, the reasons for which are unknown.

Acknowledgments

MAB, DEH and MJP thank the UTLS-Ozone NERC thematic programme for funding this work (grant number GST/02/2428). Thanks are given to Dr. A.V. Jackson and R.B. Morgan for their assistance in the HPLC analysis of the synthesised CH_3OOH.

References

[1] G.L. Vaghjiani, A.R. Ravishankara, J. Phys. Chem. 93 (1989) 1948–1959.
[2] H. Niki, P.D. Maker, C.M. Savage, L.P. Breitenbach, J. Phys. Chem. 87 (1983) 2190–2193.
[3] S.A. Penkett, B.M.R. Jones, K.A. Brice, A.E.J. Eggleton, Atmos. Environ. 13 (1979) 123–137.
[4] R.B. Morgan, A.V. Jackson, J. Geophys. Res. Atmos. 107 (2002) (Art. no. 8109).
[5] C.E. Reeves, S.A. Penkett, Chem. Rev. 103 (2003) 5199–5218.
[6] G.K. Moortgat, D. Grossmann, A. Boddenberg, G. Dallmann, A.P. Ligon, W.V. Turner, S. Gaeb, F. Slemr, W. Wieprecht, K. Acker, M. Kibler, S. Schlomski, K. Baechmann, J. Atmos. Chem. 42 (2002) 443–463.
[7] D.W. O'Sullivan, B.G. Heikes, J. Snow, P. Burrow, M. Avery, D.R. Blake, G.W. Sachse, R.W. Talbot, D.C. Thornton, A.R. Bandy, J. Geophys. Res. Atmos. 109 (2004) S13/11–S13/21.
[8] R. Sommariva, A.-L. Haggerstone, L.J. Carpenter, N. Carslaw, D.J. Creasey, D.E. Heard, J.D. Lee, A.C. Lewis, M.J. Pilling, J. Zador, Atmos. Chem. Phys. 4 (2003) 839–856.
[9] F. Ravetta, D.J. Jacob, W.H. Brune, B.G. Heikes, B.E. Anderson, D.R. Blake, G.L. Gregory, G.W. Sachse, S.T. Sandholm, R.E. Shetter, H.B. Singh, R.W. Talbot, J. Geophys. Res. Atmos. 106 (2001) 32709–32716.
[10] D.S. Cohan, M.G. Schultz, D.J. Jacob, B.G. Heikes, D.R. Blake, J. Geophys. Res. Atmos. 104 (1999) 5717–5724.
[11] M.J. Prather, D.J. Jacob, Geophys. Res. Lett. 24 (1997) 3189–3192.
[12] L. Jaegle, D.J. Jacob, W.H. Brune, I. Faloona, D. Tan, B.G. Heikes, Y. Kondo, G.W. Sachse, B. Anderson, G.L. Gregory, H.B. Singh, R. Pueschel, G. Ferry, D.R. Blake, R.E. Shetter, J. Geophys. Res. Atmos. 105 (2000) 3877–3892.
[13] R. Atkinson, D.L. Baulch, R.A. Cox, R.F. Hampson Jr., J.A. Kerr, M.J. Rossi, J. Troe, J. Phys. Chem. Ref. Data 29 (2000) 167–266.
[14] G.L. Vaghjiani, A.R. Ravishankara, J. Geophys. Res. Atmos. 94 (1989) 3487–3492.
[15] G.L. Vaghjiani, A.R. Ravishankara, J. Chem. Phys. 92 (1990) 996–1003.
[16] B.J. Finlayson-Pitts, J.N.J. Pitts, Chemistry of the lower atmosphere, in: Theory, Experiments and Applications, Academic Press, San Diego, 2000.
[17] W.B. DeMore, S.P. Sander, D.M. Golden, R.F. Hampson, M.J. Kurylo, C.J. Howard, A.R. Ravishankara, C.E. Kolb, M.J. Molina, Chemical Kinetics and Photochemical Data for Use in Stratospheric Modelling, vol. 97-4, JPL Publication, 1997.
[18] M.A. Thelen, P. Felder, J.R. Huber, Chem. Phys. Lett. 213 (1993) 275–281.
[19] A.L. Lazrus, G.L. Kok, J.A. Lind, S.N. Gitlin, B.G. Heikes, R.E. Shetter, Anal. Chem. 58 (1986) 594–597.
[20] M.A. Blitz, D.G. Johnson, M. Pesa, M.J. Pilling, S.H. Robertson, P.W. Seakins, J. Chem. Soc., Faraday Trans. 93 (1997) 1473–1479.
[21] G. Inoue, H. Akimoto, M. Okuda, J. Chem. Phys. 72 (1980) 1769–1775.
[22] S.D. Brossard, P.G. Carrick, E.L. Chappell, S.C. Hulegaard, P.C. Engelking, J. Chem. Phys. 84 (1986) 2459–2465.
[23] A. Mellouki, S. Teton, G. Le Bras, Int. J. Chem. Kinet. 27 (1995) 791–805.
[24] F.P. Tully, A.T. Droege, Int. J. Chem. Kinet. 19 (1987) 251–259.
[25] T.J. Wallington, R. Liu, P. Dagaut, M.J. Kurylo, Int. J. Chem. Kinet. 20 (1988) 41–49.
[26] L.J. Bremner, M.G. Curtis, I.C. Walker, J. Chem. Soc., Faraday Trans. 87 (1991) 1049–1055.